J. Fluid Mech. (1976), *vol.* 76, *part* 1, *pp.* 35–64
Printed in Great Britain

Axially symmetric turbulent boundary layers on cylinders: mean velocity profiles and wall pressure fluctuations

By W. W. WILLMARTH, R. E. WINKEL, L. K. SHARMA
Department of Aerospace Engineering, University of Michigan, Ann Arbor
AND T. J. BOGAR
Department of Physics, Westminster College, Pennsylvania

(Received 22 September 1975)

Experimental measurements of the mean velocity profiles produced by axially symmetric turbulent boundary layers on cylinders of various diameters are described. The profile measurements were made with very small hot wires developed for this investigation. Measurements of the wall shear stress on cylinders ranging from 0·02 to 2·0 in. in diameter are also reported. In the boundary layer on cylinders, well-defined regions exist in which the two-dimensional law of the wall and a three-dimensional wake law are valid. There was no evidence that the boundary layer was not fully turbulent even on the cylinders of smallest diameter. Measurements of wall pressure fluctuations beneath the boundary layer on a 1 in. diameter cylinder are also described. The results were much the same as those previously reported by Willmarth & Yang (1970) for a 3 in. diameter cylinder. The only difference was the discovery that the wall pressure was correlated in the transverse direction approximately half-way around the cylinder. This was not true on the 3 in. diameter cylinder.

1. Introduction

This paper reports measurements of mean velocity, wall shear stress and wall pressure fluctuations associated with the turbulent boundary layer which develops on the surface of slender circular cylinders aligned with the flow. The present measurements extend our previous experimental studies of the effect of transverse curvature on the mean flow field in turbulent boundary layers (Willmarth & Yang 1970) to boundary layers whose thickness δ is as much as 40 times the cylinder radius a. The previous measurements of wall pressure fluctuations by Willmarth & Yang (1970) for $\delta/a \simeq 2$ have also been repeated but for a larger value of δ/a of approximately four.

It is known that, near the surface in a laminar boundary layer on a slender circular cylinder, the mean velocity is proportional to the logarithm of $a+y$, where y is the distance from the surface (Glauert & Lighthill 1955). The logarithmic velocity profile is caused by the constancy of the shearing force [$\mu dU/dy$ times the cylinder circumference $2\pi(a+y)$] near the solid boundary, where the

fluid acceleration is negligible. Near the surface of cylinders of small diameter, the logarithmic profile is very 'full' compared with the Blasius profile, which is produced in a two-dimensional flow.

The tendency towards increased shear stress near the wall exhibited by a 'full' velocity profile that is caused by transverse curvature is also observed when the boundary layer is turbulent. When turbulence is present the turbulent structure is also affected by the increased shear near the wall.

Willmarth & Yang (1970) found that the power spectral density of the wall pressure fluctuations at high frequencies was larger than that beneath flat-plate boundary layers. They attributed this to an increased intensity of small-scale motion near the wall caused by the increased shearing of the turbulent eddies in the very 'full' mean velocity profile near the wall. Their space–time correlation measurements of wall pressure fluctuations also revealed that in a boundary layer with transverse curvature the intensity and lifetime of the largest-scale turbulent eddies were reduced compared with those of large-scale turbulent eddies in a flat-plate boundary layer. They attributed the change in large-scale structure to the geometry of the flow, in which, for large transverse curvature, the transverse extent of all large eddies within the boundary layer must be limited by the presence of the free stream all around the cylinder to scales of the the order of δ.

Only two previous experimental studies of the mean flow field in which the ratio δ/a was greater than two are known to the authors: Richmond (1957) and Rao & Keshavan (1972). Simultaneous measurements of the mean velocity profile and of the wall shear stress comparable in completeness and accuracy to those available for the plane boundary layer do not exist. This is due to the extreme difficulty of the experimental measurements when δ/a is large. The present measurements were designed to provide new information for large values of δ/a and to improve our understanding of the effects of transverse curvature on turbulent structure.

With regard to the mean flow field, there have already been numerous attempts to make empirical predictions about the effects produced by a large degree of transverse curvature. Richmond (1957) has proposed that the similarity embodied in Coles' (1955) streamline hypothesis for a plane boundary layer should be valid near the cylinder surface. Yu (1958) has ordered his mean velocity data, for δ/a less than two, in a different (but consistent) form. There have been a number of different semi-empirical theories, formulated by Reid & Wilson (1963), Cebeci (1970), White (1972), Chase (1972), White, Lessmann & Christoph (1973) and Patel (1973), which these writers propose can be used to predict the mean flow field in the boundary layer on a cylinder.

Rao (1967) proposed a certain similarity law for the mean velocity and has suggested, in agreement with his proposed similarity law, that as a/δ becomes small the thickness of the viscous sublayer relative to the cylinder radius increases. Patel (1973) has predicted that the flow along cylinders whose radius is so small that the dimensionless cylinder radius $a^+ = aU^*/\nu$ is less than 28 will not be fully turbulent. Here ν is the kinematic viscosity and U^* is the friction velocity, the square root of the ratio of wall shear stress to fluid density. Patel's

prediction is based upon his suggestion that the effects of favourable pressure gradient and of transverse curvature are similar.

The predictions of Rao (1967) and Patel (1973) are discussed and compared with observations in the body of the paper. We have presented our measurements in a form that appears to us to be physically significant and conceptually simple. We have made no attempt to perform a detailed comparison of our data with semi-empirical predictions of the mean flow field.

2. Experimental apparatus

In order that large values of the ratio of boundary-layer thickness to cylinder radius can be realized it is necessary to perform experiments with large values of the ratio of cylinder length to diameter. This makes it necessary to ensure that the axis of the cylinder is very straight and parallel to the flow.

2.1. *Vertical wind tunnel*

To satisfy these requirements we have designed and constructed a vertical wind tunnel in which a uniform flow is developed in a duct 18·3 ft long with an octagonal cross-section 1 ft wide. Figure 1 is a sketch of this vertical tunnel. The tunnel is fitted with a removable door extending the full length of the duct (not shown). Figure 1 shows a cylinder 1 in. in diameter mounted in the centre of the duct and extending upwards through the contraction section, whose contraction area ratio is 9:1, into the settling chamber. Further information about the vertical wind tunnel is available in Willmarth *et al.* (1975).

The vertical wind tunnel is designed such that two of the opposing walls of the octagonal duct are slightly divergent. These were adjusted to produce a uniform streamwise pressure distribution in the empty duct. The resulting velocity distribution is uniform to within 2 % of the mean velocity. The corresponding variation of the ratio of static-pressure perturbation to mean dynamic pressure is 4 %. The mean flow speed in the tunnel can be varied from zero to 250 ft/s. The turbulence level in the centre of the empty duct was not measured. However, at the 18·3 ft station with a cylinder $\frac{1}{8}$ in. in diameter installed the root-mean-square streamwise velocity was of the order of 0·5 % of the free-stream velocity at $y/\delta \simeq 1{\cdot}0$.

The boundary layer on the inner walls of the octagonal duct was turbulent at the exit of the duct, where the majority of the measurements of the velocity profile and wall pressure were performed. In the case of the cylinder 2 in. in diameter the boundary layer on the wall and on the cylinder were just beginning to merge at the duct exit. For models of smaller diameter the cylinder boundary layer did not encounter the wall boundary layers.

2.2. *Cylindrical models and flow symmetry*

The cylindrical models used in the test programme were constructed in two ways. The models with larger diameters of 1 and 2 in. were made from various short lengths of commercially available aluminium-alloy tubing with a wall

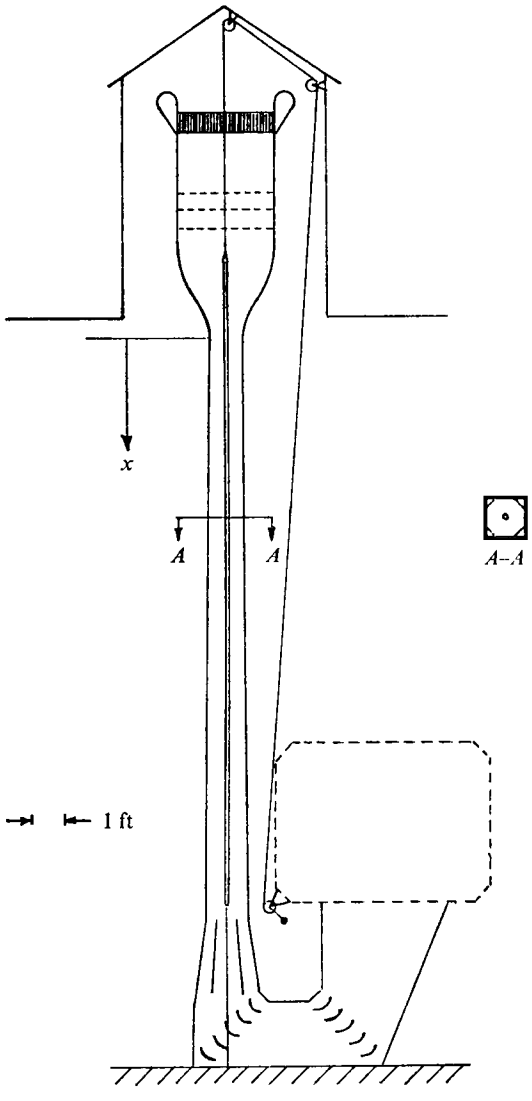

FIGURE 1. Sketch of vertical tunnel.

thickness of the order of 0·05 in. The ends of each length of tubing were machined to accept short lengths of tubing of smaller diameter, which were slipped inside each end in order to join and align the longer tubes. The assembly was held together by a taut steel cable inside the tubes that was attached to the top and bottom sections of the cylinders.

The models with smaller diameters of $\frac{1}{2}$ and $\frac{1}{4}$ in. were made from single lengths of stainless-steel tubing. The models with the smallest diameters, $\frac{1}{8}$, 0·040 and 0·020 in., were made from solid stainless-steel rods. The stainless-steel models were not initially straight. Straightening was achieved by suspending them from the ceiling in the laboratory and heating them to a red heat (by passing electric current along them) while a weight was fastened to their lower end.

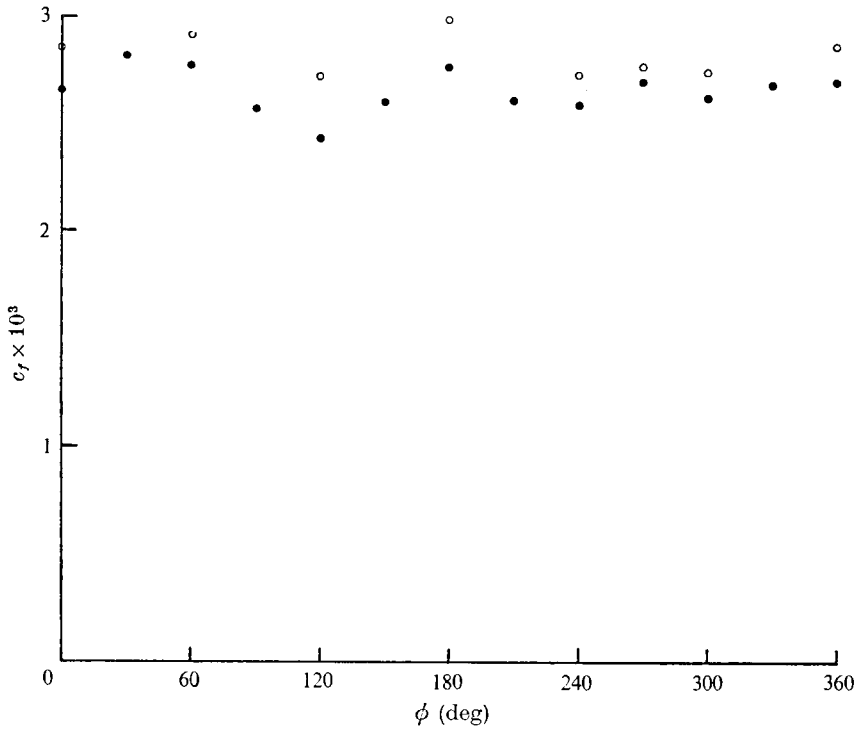

FIGURE 2. Variation of the skin-friction coefficient with azimuthal angle on the surface of the 1 and 2 in. cylinders. ○, $a = 0{\cdot}5$ in., $U_\infty = 155{\cdot}4$ ft/s, $Re_\theta = 2{\cdot}23 \times 10^4$, $x = 18{\cdot}3$ ft; ●, $a = 1{\cdot}0$ in., $U_\infty = 154{\cdot}2$ ft/s, $Re_\theta = 1{\cdot}76 \times 10^4$, $x = 18{\cdot}3$ ft.

No attempt was made to trip the boundary layer on any of the cylinders. We adopted this procedure to avoid introducing long lasting, possibly large-scale turbulent eddies which would not normally occur. As discussed later in the paper (see also our previous work, Willmarth & Yang 1970), the effect of transverse curvature is to reduce the spatial scale of the turbulence. The location of the transition point was not determined on any of the cylinders.

Considerable difficulty was experienced in properly aligning the 1 and 2 in. cylindrical models in the duct such that the boundary-layer profiles were approximately symmetrical. The best arrangement of these models was obtained when they were mounted on the centre-line of the octagonal duct. The variation of the velocity around the 2 in. cylinder measured with an eight-tube rake at a distance of $y = 0{\cdot}327$ in. from the wall was determined to be of the order of 10 % of the stream velocity.

We also measured the variation of the wall shear stress around the 2 and 1 in. cylinders using a Preston tube. In these measurements, shown in figure 2, the variation of the wall shear stress was of the order of 10 % of the mean wall shear stress. The measurements were made by rotating each cylinder, which had a single Preston tube attached to its surface. The use of the Preston tube for measurements of wall shear stress on cylinders is discussed in detail in §3.1. What is emphasized here is the degree of flow symmetry about the cylinder.

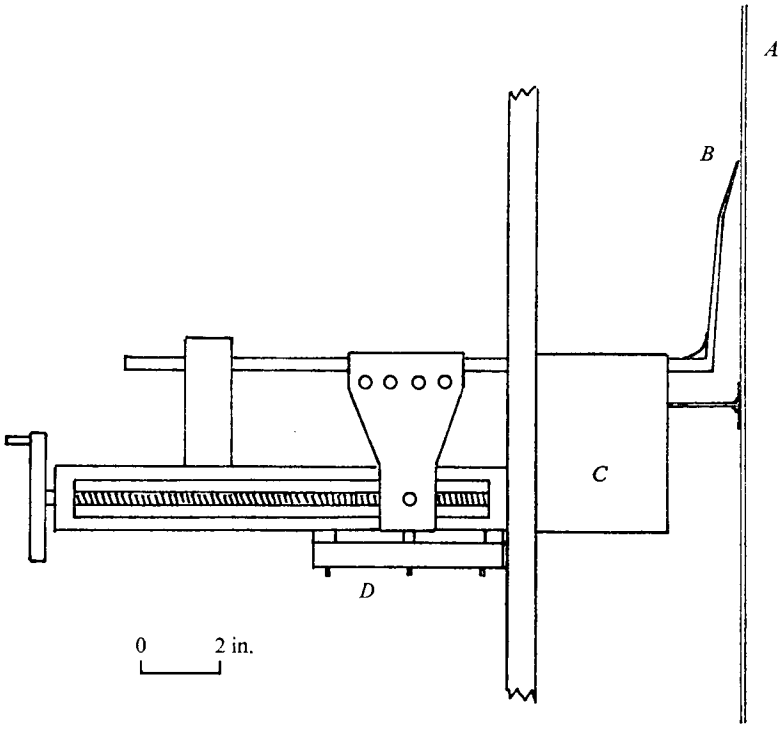

FIGURE 3. Sketch of hot-wire probe and traversing mechanisms. *A*, cylinder; *B*, hot-wire probe; *C*, streamlined strut; *D*, linear potentiometer used to sense position of hot-wire probe.

In general, it was found that 1 and 2 in. cylinders were not as uniform and straight as the models of smaller diameter. For the smaller, stainless-steel models it was determined, with a rotatable impact pressure probe, that the symmetry of the boundary layer was excellent. The greatest variation in velocity was no more than 4 % of the free-stream velocity on the $\frac{1}{4}$ in. model and was 1 % or less on the other models. These results suggest that a cylinder must be straight to within a small fraction of its diameter in order that reasonably axially symmetric flow on it can be obtained.

2.3. *Instrumentation for measurements of the mean velocity profiles*

The initial measurements of the mean velocity were made on the 1 and 2 in. cylinders using an impact pressure probe. The rectangular probe opening was 0·003 in. high and 0·045 in. wide. The traversing mechanism was mounted entirely inside the cylinder and this restricted the motion of the probe to distances of less than $\frac{1}{2}$ in. from the surface. For measurements at greater distances a rake consisting of a number of impact pressure probes was mounted on the cylinder. Measurements of the mean velocity near the wall for values of $yU^*/\nu = y^+$ less than 15 were not possible with the impact pressure probe.

Mean velocity measurements on the smaller diameter, stainless-steel cylinders were made using a small hot-wire anemometer probe mounted on an external

traversing mechanism. Figure 3 shows a sketch of the arrangement that was used to support the cylinder and traverse the probe. The probe was positioned by a lead screw driving a nut attached to the probe. The probe position was sensed with a linear potentiometer attached to the traversing nut. The probe position and hot-wire output were displayed on an x, y plotter.

Measurements of mean velocity on cylinders of small diameter are not accurate near the surface unless very small hot-wire probes are used. The hot-wire length must be much less than the radius of the cylinder in order to avoid spatial averaging of the mean velocity on the cylindrical stream surfaces coaxial with the cylinder. The hot-wire diameter must also be small in comparison with the distance from the wall, in order that the conductive heat loss to the wall is small.

We have developed and used very small hot wires with a diameter of $0{\cdot}5\,\mu$m and length of the order of $100\,\mu$m. The construction of the wires is described in the appendix. A photograph taken using a scanning electron microscope of a typical hot wire is shown in figure 4 (plate 1).

Information about static and dynamic calibration and the associated constant-temperature electronic system for the small hot wires is contained in Willmarth *et al.* (1975).

2.4. *Instrumentation for measurements of wall pressure fluctuations*

The configuration of the piezoelectric pressure transducers and electronic system used for measuring the wall pressure fluctuations is described in detail by Willmarth *et al.* (1975). This configuration was similar to that used by Willmarth & Yang (1970). The diameter of the sensitive area of the transducers was 0·06 in. Twelve transducers were mounted flush with the surface of a 1 in. cylinder and arranged with spacings calculated to maximize the number of measurable spatial correlations.

3. Measurements of mean velocity profiles

Measurements of the mean velocity profiles on cylinders with diameters ranging from 2·0 to 0·020 in. are reported in this section. In conjunction with the velocity profiles we also measured the wall shear stress using two different methods described below. The velocity profile measurements are presented in terms of a wall region and a wake region.

3.1. *Measurements of wall shear stress using a Preston tube*

A Preston tube, a circular impact pressure tube in contact with the surface, was used to measure the wall shear stress on the cylinders of larger diameter. The use and calibration of the Preston tube were reported by Preston (1954). In order to use a Preston tube to measure the shear stress on a cylinder it is necessary either to calibrate the tube in the boundary layer on the cylinder or to verify that the flat-plate calibration data are valid there. We have been able to show that the flat-plate calibration data can be used on the cylinders of larger diameter that were used in our investigation.

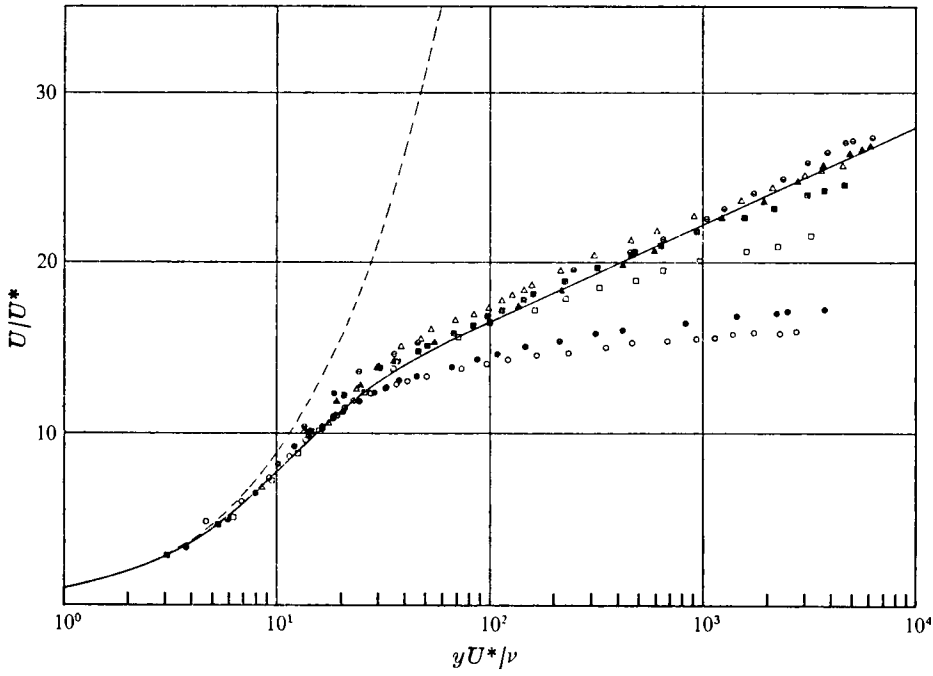

FIGURE 5. Seven representative velocity profiles in wall co-ordinates showing the influence of increasing transverse curvature. ——, flat plate, Coles (1955); - - -, equation (11), $a^+ = 33{\cdot}4$.

	⊖	▲	△	■	□	●	○
a (in.)	1·0	0·5	0·25	0·125	0·063	0·02	0·01
δ/a	1·8	4·1	4·7	9·4	16·0	27·0	37·5

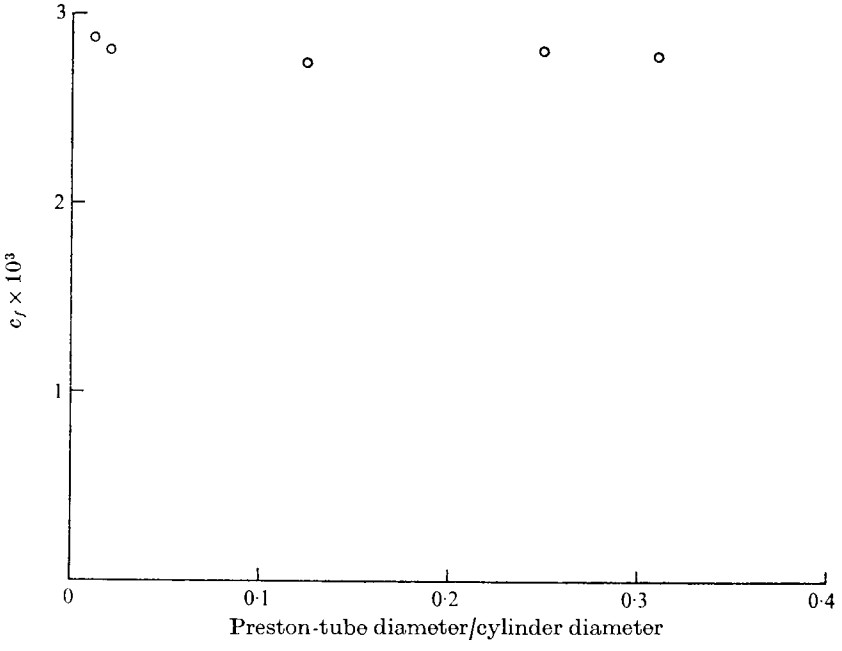

FIGURE 6. Measurements of skin-friction coefficient using Preston tubes of various diameters on a 1 in. cylinder. $U_\infty = 154$ ft/s, $\theta = 0{\cdot}304$ in., $Re_\theta = 2{\cdot}23 \times 10^4$, $x = 18{\cdot}3$ ft, $\delta/a = 4.1$.

Data set	d (in.)	x (ft)	U_∞ (ft/s)	Hot-wire length (in.)	δ (in.)	δ^* (in.)	θ (in.)	$R_a = Ua/\nu$	Re_θ	U^* (ft/s) by fitting	c_f
1	0·020	18·3	96	0·005	0·425	0·0735	0·0630	482	$3·04 \times 10^3$	6·65	$9·59 \times 10^{-3}$
2	0·020	18·3	147	0·005	0·375	0·0692	0·0591	736	$4·35 \times 10^3$	9·20	$7·84 \times 10^{-3}$
3	0·020	18·3	180	0·005	0·240	0·0429	0·0327	899	$2·95 \times 10^3$	11·30	$7·89 \times 10^{-3}$
4	0·040	18·3	145	0·005	0·540	0·0791	0·0752	1439	$5·41 \times 10^3$	8·40	$5·71 \times 10^{-3}$
5	0·125	18·3	142	0·005	1·000	0·1780	0·1530	4330	$1·06 \times 10^4$	6·50	$4·18 \times 10^{-3}$
										Preston tube	
6	0·250	18·3	104	0·019	1·302	0·2418	0·2237	6203	$1·11 \times 10^4$	4·56	$3·83 \times 10^{-3}$
7	0·250	18·3	160	0·019	1·181	0·2042	0·1896	9494	$1·44 \times 10^4$	6·55	$3·34 \times 10^{-3}$
8	0·250	18·3	198	0·019	1·165	0·1779	0·1657	11693	$1·55 \times 10^4$	7·73	$3·04 \times 10^{-3}$
9	0·500	18·3	105	0·040	1·380	0·2233	0·1994	12790	$1·02 \times 10^4$	4·216	$3·20 \times 10^{-3}$
10	0·500	18·3	159	0·040	1·178	0·1767	0·1573	19230	$1·21 \times 10^4$	6·211	$3·04 \times 10^{-3}$
11	0·500	18·3	192	0·040	1·159	0·1703	0·1537	23100	$1·42 \times 10^4$	7·4087	$2·98 \times 10^{-3}$
12	1·000	18·3	155	Impact pressure	2·062	0·3460	0·3040	36680	$2·23 \times 10^4$	5·75	$2·74 \times 10^{-3}$
13	2·000	18·3	158	Impact pressure	1·760	0·2770	0·2370	74260	$1·76 \times 10^4$	5·765	$2·64 \times 10^{-3}$
14	2·000	18·3	204	Impact pressure	1·880	0·2940	0·2340	92310	$2·16 \times 10^4$	6·979	$2·34 \times 10^{-3}$

TABLE 1. Summary of data for all cylinders

The use and calibration of the Preston tube (Preston 1954; Patel 1965) are based on the assumption that the tube is entirely immersed in the wall region of the flat-plate boundary layer, where the law of the wall is valid. If a Preston tube is to give an accurate measurement of the wall shear stress on a cylinder one requires that the cylinder velocity profile should coincide with the flat-plate law of the wall and that the Preston tube's diameter should be small compared with the cylinder diameter. For cylinder diameters of 2, 1, 0·5 and 0·25 in. the velocity profile does coincide with the flat-plate law of the wall over a considerable portion of the boundary layer; see figure 5. To determine how small the diameter of the Preston tube should be compared with the cylinder diameter we installed Preston tubes of various diameters on the surface of the 1 in. cylinder. These Preston tubes were all well within the portion of the cylinder velocity profile which coincides with the flat-plate law of the wall. The wall shear stress obtained using the flat-plate calibration data of Patel (1965) was expected to approach a constant value as the ratio of Preston-tube diameter to cylinder diameter became small. Our measurements, shown in figure 6, indicate that the shear stress obtained from all the Preston tubes was the same (i.e. within the experimental scatter) for ratios of Preston-tube diameter to cylinder diameter less than 0·3.

One may conclude that, if the Preston tube has a diameter less than 0·3 times the cylinder diameter and also lies within the region of the cylinder velocity profile described by the flat-plate law of the wall, one can use the flat-plate calibration of Patel (1965) to determine the wall shear stress on the cylinder. To be somewhat conservative we restricted the Preston-tube diameter to less than 0·16 times the cylinder diameter when measuring wall shear stress by this method.

We used two Preston tubes of small diameters of 0·02 and 0·04 in. to determine the wall shear stress on the 2, 1, 0·5 and 0·25 in. cylinders. The results are displayed in table 1. We were not confident about the validity of Preston-tube measurements of wall shear stress on cylinders of very small diameter since the region coincident with the flat-plate law of the wall then becomes very small; see figure 5. Another method, described below, was developed for the smaller cylinders. The shear stresses measured by the two methods were in agreement for the cylinders of larger diameter.

3.2. *Measurements of wall shear stress using small hot wires*

A method to measure directly the mean velocity gradient near the wall, and thereby deduce the wall shear stress, was developed for use with cylinders of very small diameter. The method employed a very short hot wire of small diameter which could be positioned and traversed accurately ($\pm$ 0·0005 in.) to within 0·001 in. from the surface of the cylinder; see figure 3.

In order that accurate mean velocity measurements can be made near the wall on cylinders of small diameter, it is necessary that the hot wire be very short compared with the cylinder radius. If the hot-wire length is not small compared with the cylinder radius the wire will be exposed to a variation in velocity along its length. In general, the wire will indicate too high a velocity relative to the velocity at the centre, where the mean velocity is a minimum on that portion of the wire nearest the wall.

When the hot wire is very near the wall, there will also be an appreciable loss of heat caused by conduction to the cold wall. The increased heat loss to the wall is interpreted as an increase in the fluid velocity as the hot wire approaches the wall. According to Wills (1962) the error in velocity caused by heat conduction to the wall is negligible when the wire is of the order of 100 diameters from the wall. The hot wires used in this investigation were approximately 0·004 in. (100 μm) long and 0·00002 in. (0·5 μm) in diameter and were made from platinum wire drawn by the Wollaston process (a photograph is shown in figure 4).

Using the small hot wire, the mean velocity profile on small cylinders was measured to distances of the order of 0·001 in. from the surface. At this distance the error caused by heat conduction to the wall is negligible. Accurate measurement of the absolute distance of the wire from the cylinder surface was not attempted. This would have required construction of a large rigid probe support and the use of a high-power microscope inside the vertical tunnel since the wire diameter (0·5 μm) is comparable to the wavelength of visible light. We were able to use a small telescope to make gross observations of the position of the wire's supporting prongs from outside the tunnel while the tunnel was operating. It was possible to observe the approximate position of the wire near the wall but not with the absolute accuracy required for direct shear stress measurements. To measure the shear stress we developed a method (described below) for extrapolation of velocity profile data to the wall.

The technique is based upon the observation that very near the wall, where $y/a \ll 1$, the region of the cylinder boundary layer within and just above the sublayer obeys the law of the wall and has the same velocity profile as is found in the flat-plate boundary layer. The observation was verified by measuring the wall shear stress and the velocity profile on the 2, 1, $\frac{1}{2}$ and $\frac{1}{4}$ in. cylinders. For these larger cylinders U^* was determined from Preston-tube measurements as described above. When these data are plotted in wall co-ordinates, see figure 5, one observes that for cylinders with diameters in the range $\frac{1}{4}$–2 in. there is a well-defined profile near the wall which agrees in each case with the two-dimensional law of the wall.

The technique for measuring the wall shear stress from the velocity profile required first that the hot-wire system's output voltage be calibrated in terms of the velocity of the free stream. This was done by positioning the wire well outside the boundary layer and then adjusting the tunnel speed to various known values. The tunnel speed was then fixed at the desired speed of the free stream and the wire was positioned as close to the surface as possible. The hot wire was then slowly traversed away from the surface. The voltage from the linear potentiometer indicating the relative position of the hot wire and the hot-wire system's output voltage were recorded on an x, y recorder. From these data and the hot-wire calibration data a plot of wire position *vs.* mean velocity was obtained. At the point nearest the wall the mean velocity was of the order of $\frac{1}{4}$ to $\frac{1}{5}$ of the free-stream velocity.

At the data points nearest the wall the second derivative $\partial^2 U/\partial y^2$ was slightly less than zero, so that precise determination of the wall shear stress was not possible by fairing a straight line through the data. Instead we used a graphical

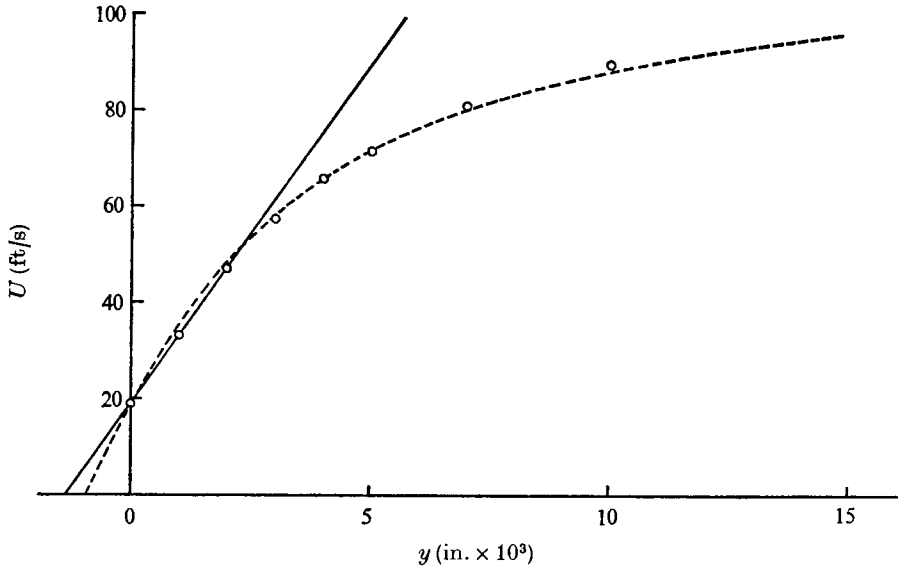

FIGURE 7. Plot of mean velocity measured by hot wire as a function of distance from the wall for $\frac{1}{8}$ in. cylinder. ——, straight line, $U^* = 5{\cdot}33\,\text{ft/s}$; - - -, two-dimensional law of the wall, $U^* = 6{\cdot}5\,\text{ft/s}$.

procedure to determine both the y origin (absolute position of the wire) and the wall shear stress by requiring that the velocity data nearest the wall coincided with the two-dimensional law of the wall as tabulated by Coles (1955).

A typical example illustrating the quality of the data and the accuracy of this method is displayed in figure 7. In this figure the original data for the $\frac{1}{8}$ in. cylinder are shown as points at which the voltage read from the x, y plotter output is converted to velocity and relative position using the calibration data. The y co-ordinate in figure 7 has been made zero for the point nearest the wall. The straight line is faired through the last two data points. This indicates the best estimate of wall shear stress and absolute location of the wall relative to the hot wire that can be obtained by assuming $\partial^2 U/\partial y^2 = 0$ for the last two data points. The values of U^* and the absolute location y_0 of the wall relative to the data point nearest the wall determined by this method were $5{\cdot}33\,\text{ft/s}$ and $1{\cdot}3 \times 10^{-3}$ in. respectively.

The derivative $\partial^2 U/\partial y^2$ is slightly negative even for the points nearest the wall. We thus assumed that the two-dimensional law of the wall was valid. The dashed line in figure 7 shows the velocity profile predicted from tabulated values of the two-dimensional law of the wall (Coles 1955) when the values of U^* and y_0 are adjusted to fit all the data points shown on the plot. These values of U^* and y_0 were $6{\cdot}5\,\text{ft/s}$ and $0{\cdot}95 \times 10^{-3}$ in. respectively. Similar results were obtained for cylinders of smaller diameter. All the measurements of U^* and y_0 for the smaller cylinders were determined by requiring agreement with the law of the wall for the data points nearest the wall. We also performed checks on this method by comparison with the Preston-tube determination of wall shear stress described in §3.1 for the $\frac{1}{2}$ and $\frac{1}{4}$ in. cylinders and found good agreement ($\pm 5\,\%$).

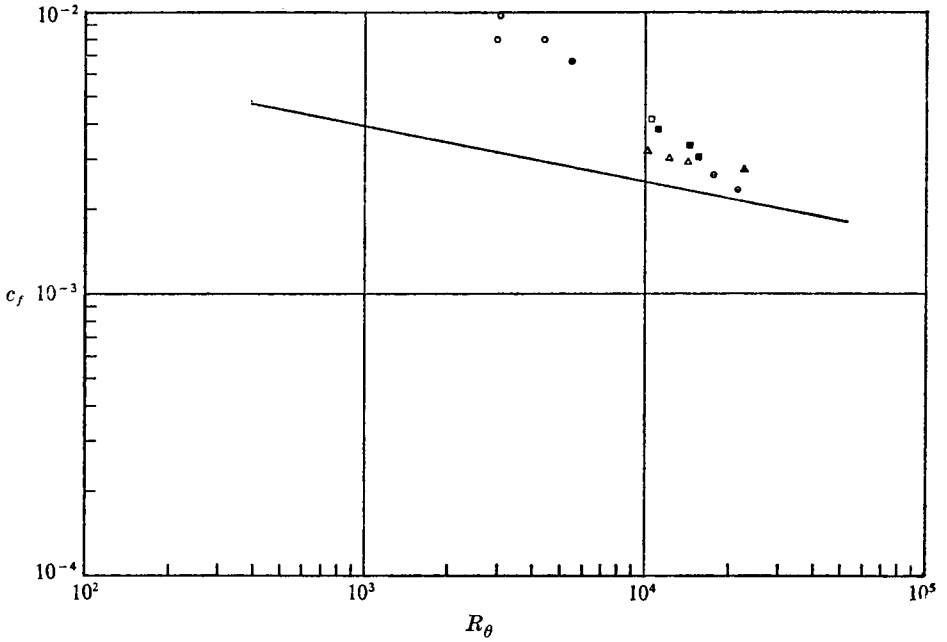

FIGURE 8. Measured turbulent skin-friction coefficient as a function of Re_θ for various cylinder diameters; see table 1 for other boundary-layer properties corresponding to these values of skin friction and Re_θ.

To illustrate the difficulty of direct shear stress measurements based on the velocity profile we remark that the absolute accuracy in measuring the position of the hot wire relative to the cylinder surface must be of the order of $\pm 10^{-5}$ in. for measurements of shear stress within $\pm 5\,\%$. Furthermore the linear portion of the velocity profile extends outwards only a distance of the order of 10^{-4} in. This is of the order of 5 hot-wire diameters, and velocity measurements at this distance from the wall would require large corrections for the effect of heat conduction to the wall.

The accuracy of the present shear stress measurements is probably only ± 10 or $15\,\%$ since, in addition to the errors in measurement, there are also errors which are not well documented that are caused by asymmetry in the flow about the cylinder. These errors are greatest for the 1 and 2 in. cylinders (see figure 2), which were not as straight as the cylinders of smaller diameter.

The shear stress measurements have been plotted as a function of the Reynolds number Re_θ based on momentum thickness in figure 8. The momentum thickness θ is defined by the expression

$$(\theta + a)^2 - a^2 = \int_{a^2}^{(a+\delta)^2} (1 - U/U_\infty)\,(U/U_\infty)\,dr^2 \tag{1}$$

and the displacement thickness δ^* by

$$(\delta^* + a)^2 - a^2 = \int_{a^2}^{(a+\delta)^2} (1 - U/U_\infty)\,dr^2; \tag{2}$$

see Moore (1952).

3.3. *Velocity profile measurements and the law of the wall*

The law of the wall for a turbulent boundary layer requires that in the region near the wall the mean velocity is a function of the distance from the wall, the friction velocity and the kinematic viscosity, namely

$$U/U^* = f(yU^*/\nu). \tag{3}$$

In a boundary layer with transverse curvature the inclusion of an additional length scale represented by the radius of curvature of the surface results in an extended law of the wall of the form

$$U/U^* = g(yU^*/\nu, y/a). \tag{4}$$

This implies that the flow in the outer part of the boundary layer can affect the wall region only through changes in the friction velocity U^*. We may combine (4) with the well-known principle from boundary-layer theory that on a curved surface the two-dimensional approximations to the equations of motion are valid if the thickness of the viscous region is small compared with the radius of surface curvature. Therefore, near the wall in the boundary layer on a cylinder there must be some range of the extended law of the wall (4) which coincides with the two-dimensional law of the wall (3) when $y/a \ll 1$. This behaviour was observed and used in § 3.2 above and is further discussed below.

In the present experiments we were not able to perform measurements of mean velocity profiles for a sufficient number of cylinder diameters nor for sufficient different values of U^* to deduce accurately the extended law of the wall in the form given by (4). An equivalent form of the extended law of the wall is

$$U/U^* = h(yU^*/\nu, aU^*/\nu). \tag{5}$$

The parameters of all the boundary-layer profiles that were measured are tabulated in table 1. Tables of the complete velocity profile data are available in Willmarth *et al.* (1975). We have plotted selected velocity profile data in the form suggested by (5) in figure 5. It can be observed in figure 5 that the profiles for cylinders with diameters between 2 and $\frac{1}{8}$ in. agree with one another and with the two-dimensional law of the wall for a large range of y^+. As the cylinder diameter is reduced below $\frac{1}{8}$ in. the profiles begin to depart from each other and from the two-dimensional law of the wall at smaller and smaller values of y^+. However, for still smaller values of y^+, very near the wall, the profiles continue to adhere to the two-dimensional law of the wall. This is in accordance with the above discussion, in which two-dimensionality of the flow is expected when the ratio of distance from the wall to radius of surface curvature is small.

3.4. *Velocity profile measurements and the law of the wake or defect law*

From the geometry of the boundary-layer flow on a cylinder it is apparent that, as the cylinder radius decreases, the perimeter of the boundary layer adjacent to the wall becomes small compared with the perimeter at $y = \delta$, adjacent to the free stream. This suggests that when δ/a is large the wakelike outer portion of the

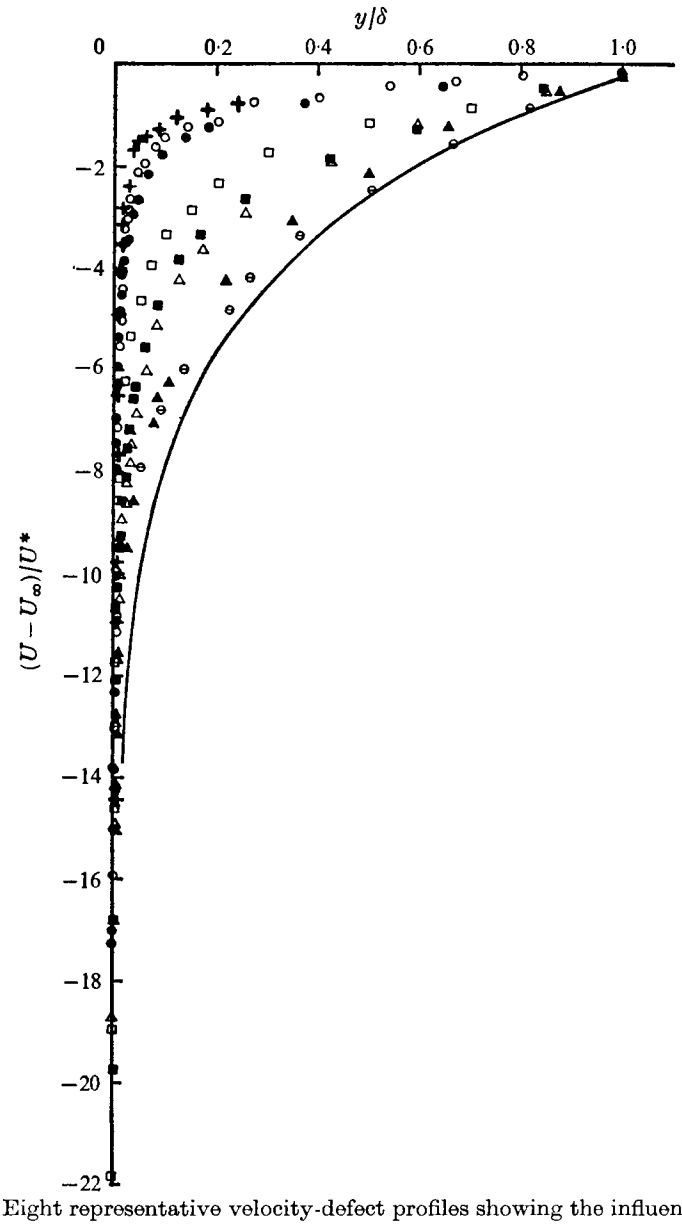

FIGURE 9. Eight representative velocity-defect profiles showing the influence of increasing transverse curvature. ——, flat plate, Clauser (1956).

	⊖	▲	△	■	□	●	○	+
a (in.)	1·0	0·5	0·25	0·125	0·063	0·02	0·01	0·01
δ/*a*	1·8	4·1	4·7	9·4	16·0	27·0	37·5	42·5

mean velocity profile should have a structure quite independent of the wall region and that it should be an important part of the mean flow field.

Despite our deduction that the wakelike component of the boundary-layer flow (see Coles (1956) for a two-dimensional formulation) is an important part of the boundary layer on a cylinder, we are faced with the paradox that, as the

cylinder radius first decreases, almost the entire profile apparently obeys the two-dimensional law of the wall for values of $\delta/a < 10{\cdot}4$; see figure 5. For cylinders of smaller radii departures from the logarithmic law become apparent. The wake-like behaviour of the boundary layer on a cylinder is not as obvious as it is for the two-dimensional boundary layer, in which the profiles clearly depart from (rise above) the logarithmic portion of the law of the wall for large y^+.

We adopt the point of view, in analogy with two-dimensional flow with zero pressure gradient, that the wakelike outer flow should obey a defect law. The only influence of the wall region is that the velocity defect should scale with the friction velocity. The velocity defect then depends upon the distance from the wall and the two length scales, the boundary-layer thickness δ and the radius of curvature of the cylinder a. We have defined the boundary-layer thickness δ to be that distance from the wall at which $U = 0{\cdot}99U_\infty$. One then obtains from dimensional analysis

$$(U - U_\infty)/U^* = F(y/\delta, \delta/a). \tag{6}$$

The velocity defect has been plotted as a function of y/δ on plots similar to those used by Clauser (1956). Figure 9 displays the behaviour of the velocity defect for a representative set of eight profiles with values of δ/a ranging from 1·8 to 42·5. For large δ/a the profiles are very full with a small velocity defect, as one would expect. For small values of δ/a the defect profiles approach the flat-plate universal data (shown by the solid line) that were obtained from figure 3 of Clauser (1956).

4. Measurements of wall pressure fluctuations

Wall pressure fluctuation measurements were made on the surface of the 1 in. cylinder at a distance of 18 ft from the beginning of the test section of the vertical tunnel. At this station the boundary layer was 2·06 in. thick. The ratio δ/a was 4·12, which is twice as large as that obtained in our previous measurements on a 3 in. cylinder; see Willmarth & Yang (1970). In the present investigation we repeated most of the wall pressure measurements described by Willmarth & Yang (1970) and used the same techniques and similar equipment. In the following sections we shall emphasize those features and measurements that differ from the previous work.

4.1. *Corrections for model vibration and ambient sound field in the vertical wind tunnel*

The sound level in the free stream in the vertical tunnel was somewhat larger than in the previous tests in a 5×7 ft low-speed tunnel (Willmarth & Yang 1970). This was caused by the more complex and less aerodynamically clean diffuser and turning vanes of the vertical tunnel; see figure 1. In addition to the sound field, there were unavoidable vibrations of the 1 in. cylinder, which caused extraneous signals from the pressure transducers at low frequencies. We did not attempt detailed measurements of the ambient sound and vibration field but developed a method to correct the space–time correlation measurements for the presence of these spurious signals.

The normalized wall pressure correlation is defined by

$$R_{pp}(x_1, x_3, \tau) = \frac{\overline{p(x, z, t)\, p(x + x_1, z + x_3, t + \tau)}}{[\overline{p^2(x, z, t)}\, \overline{p^2(x + x_1, z + x_3, t + \tau)}]^{\frac{1}{2}}}, \tag{7}$$

where an overbar denotes a time average and the co-ordinate z (and x_3) lies in the surface of the cylinder and is normal to the axis (and the free stream). The rejection of frequency components below 250 Hz, using a high-pass filter,† removed almost all the vibration signals. We remark that vibration of the transducer array presented a very difficult problem. We were able to reduce the vibration to a manageable level only after many months of experimental work. The remaining extraneous pressure signals, produced by the upstream propagation of sound from the diffuser, caused a small 'bump' in the space–time correlation curves for small negative time delays when the transducer separation distance was very large. The negative time delay at the centre of the 'bump' corresponds to the upstream transit time of sound waves in the free stream with velocity equal to the sound speed minus the free-stream velocity. We verified that the location of the maximum correlation at the centre of the bump moved nearer to the time origin (in proportion to the transducer separation distance) as the spatial separation of the transducers was reduced.

The removal of the free-stream sound pressure correlation was quite simple. We notice that both transducer pressure signals are the sum of a turbulent wall pressure p_T and a free-stream sound-field pressure p_s. Then the correlation between two transducer pressures at different streamwise stations 1 and 2 is

$$\begin{aligned} \overline{p_1 p_2} &= \overline{(p_{1T} + p_{1s})\,(p_{2T} + p_{2s})} \\ &= \overline{p_{1T} p_{2T} + p_{1s} p_{2s}}, \end{aligned} \tag{8}$$

assuming that the pressure fluctuations in the free-stream sound field are not correlated with the wall pressure fluctuations. A digital computer was programmed to subtract the term $\overline{p_{1s} p_{2s}}$ from the measured wall pressure correlation. The resulting turbulent pressure correlation was renormalized as required by (7) (for further information see Willmarth *et al.* 1975). The correction was applied to all the measured space–time correlations regardless of transducer separation distance or orientation since most of the energy of the sound field in the free stream is below 1000 Hz and has a large wavelength compared with the transducer separation distance.

4.2. *Streamwise space–time correlation of the wall pressure*

The measurements of the wall pressure fluctuations beneath the axially symmetric boundary layer will be presented in the light of our knowledge of wall pressure fluctuations beneath a plane, two-dimensional boundary layer. The most striking property of the wall pressure fluctuations beneath a plane boundary layer is the now well-known fact that the random pressure fluctuations are convected at speeds of the order of $0{\cdot}5U_\infty$ to $0{\cdot}85U_\infty$; see Willmarth (1975*a*). In

† Ithaco Model 4213 variable band-pass filters.

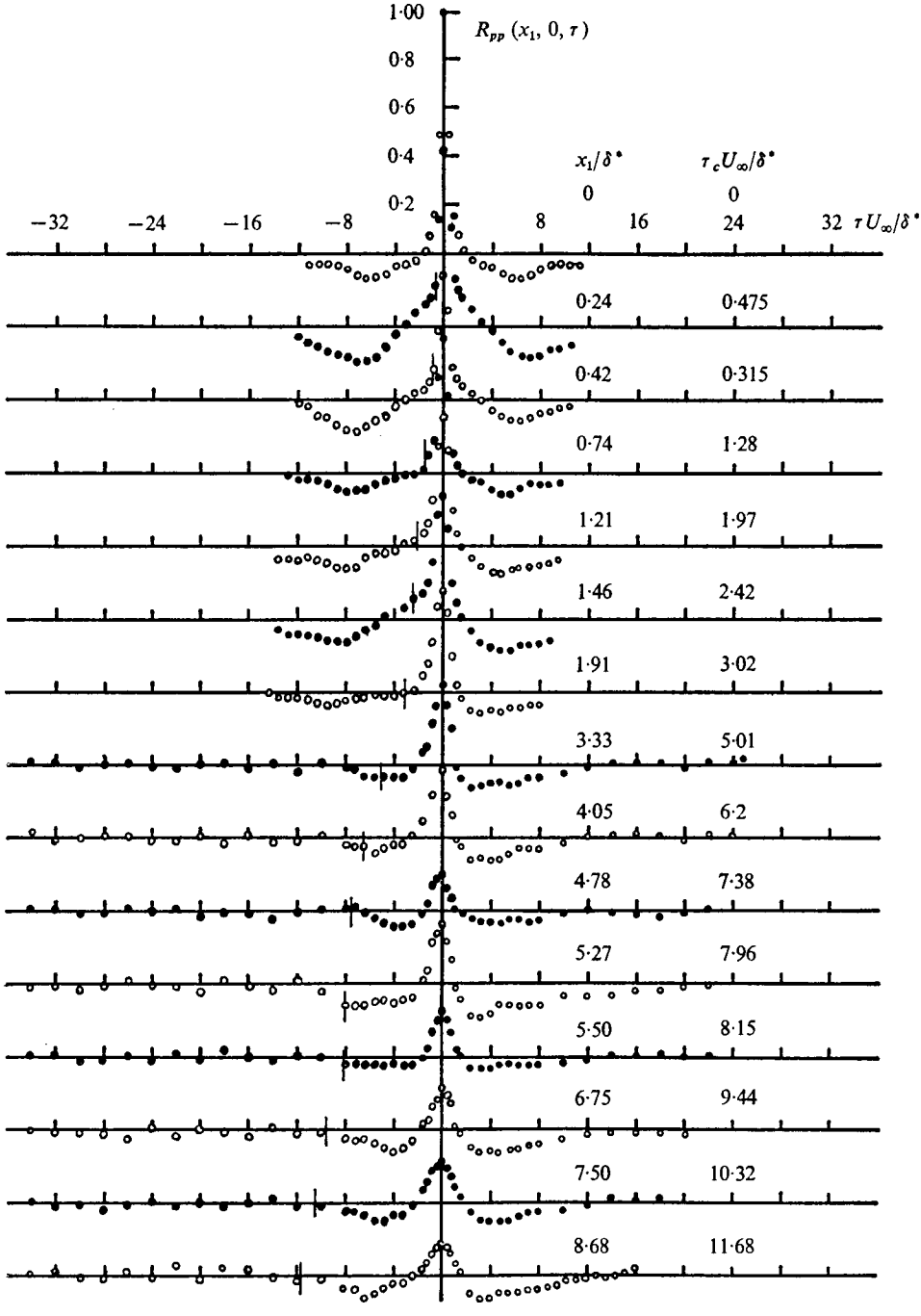

FIGURE 10. Corrected measurements of streamwise space–time correlations for various spatial separations x_1/δ^*. The small vertical line along the $-\tau \bar{U}_\infty \delta^*$ axis shows the origin $\tau = 0$ for each transducer spacing. The origin shift is given by the parameter $\tau_c U_\infty/\delta^*$.

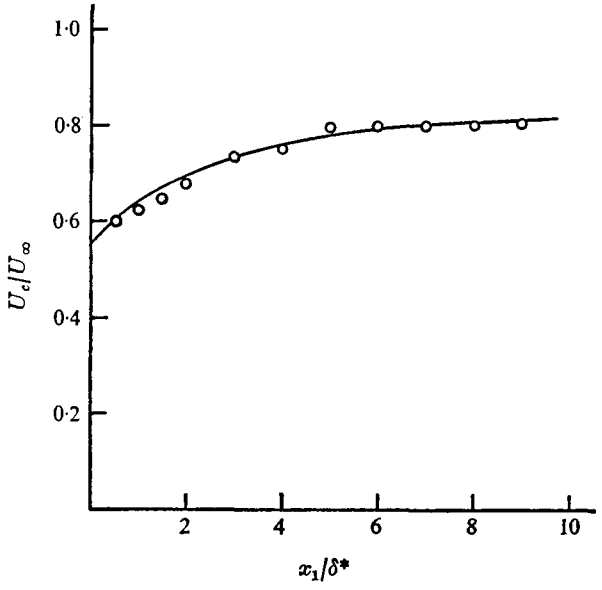

FIGURE 11. Local convection speed of pressure-producing turbulent eddies. ○, present measurements; ——, Willmarth & Yang (1970).

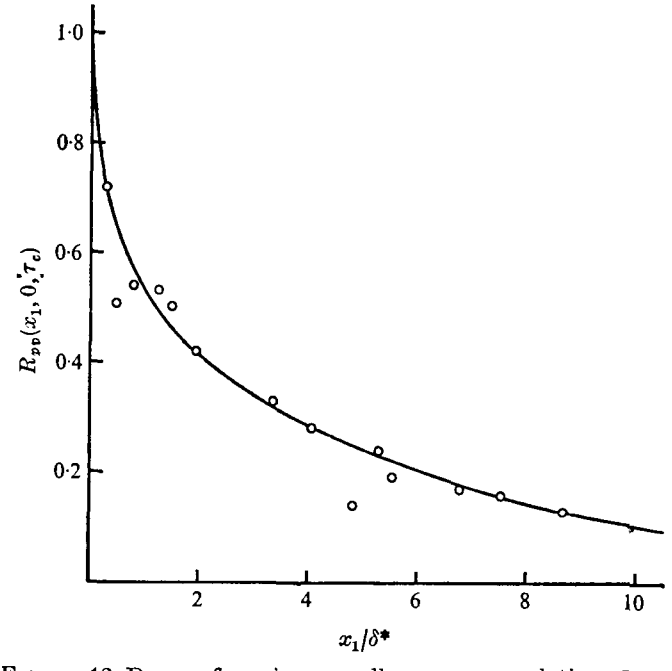

FIGURE 12. Decay of maximum wall pressure correlation. ○, present measurements, $\delta/a \simeq 4$; ——, Willmarth & Yang (1970), $\delta/a \simeq 2$.

the experiments of Willmarth & Yang (1970), with $\delta/a \simeq 2$, it was found that the space–time correlation of wall pressure fluctuations beneath a boundary layer with transverse curvature also shows convection and decay, but with the important difference that the rate of decay of the pressure correlation is more rapid. The convection velocity was the same as that beneath a plane boundary layer.

Figure 10 contains the corrected streamwise space–time correlations measured in the present investigation, with $\delta/a \simeq 4$. In these wall pressure measurements and all others reported in this paper all contributions to the pressure fluctuations with frequencies below 250 Hz have been removed with a high-pass filter. The present measurements are very much the same as those reported by Willmarth & Yang (1970). The local convection velocity of the pressure fluctuations was obtained from the slope of a line in the x_1, τ plane connecting the maximum correlations shown in figure 10. The local convection velocity is displayed in figure 11. The convection speed and its increase with increasing transducer separation x_1 are virtually the same as in a plane boundary layer and in the axisymmetric boundary layer of Willmarth & Yang (1970), with $\delta/a \simeq 2$.

Figure 12 displays the decay of the space–time correlation as one follows the trajectory of the maximum correlation in the x_1, τ plane. In this figure the peak values of R_{pp} are plotted as a function of x_1/δ^*. It can be observed that the decay is also virtually identical to that measured by Willmarth & Yang (1970). The rate of decay of the pressure correlation is accelerated in comparison with that of a plane boundary layer. For example, in a plane boundary layer the peak value of $R_{pp} = 0{\cdot}1$ occurs at $x_1/\delta^* = 22{\cdot}6$, whereas it is located at $x_1/\delta^* \simeq 10$ in the present case.

4.3. *Streamwise and lateral spatial correlations of the wall pressure*

The spatial correlations of the wall pressure (with zero time delay) have been studied to determine the contours of constant pressure correlation on the surface of the cylinder. The array of twelve pressure transducers was designed such that a large number of pressure correlations for different spatial separations could be efficiently measured with a small number of pressure transducers. All of the wall pressure correlations (at zero time delay) were measured in the frequency range $0{\cdot}257 < \omega\delta^*/U_\infty$, i.e. $f > 250$ Hz, and have been corrected for the effect of sound in the free stream.

The results of the spatial correlation measurements are displayed in figures 13–15. Figures 13 and 14 show the streamwise and lateral wall pressure correlations respectively. As reported by Willmarth & Yang (1970) the correlation decreases more rapidly with increasing x_1 or x_3 than has been observed in a plane boundary layer. There is very little difference between the present results, for $\delta/a \simeq 4$, and those of Willmarth & Yang (1970), with $\delta/a \simeq 2$, when the spatial separation is referred to the displacement thickness δ^*. However, in the present investigation, for $\delta/a \simeq 4$, the ratio of displacement thickness to cylinder radius is $\delta^*/a \simeq 0{\cdot}69$ whereas it was only $\delta^*/a \simeq 0{\cdot}29$ in the experiments of Willmarth & Yang (1970), with $\delta/a \simeq 2$. The result of this is that the surface pressure fluctua-

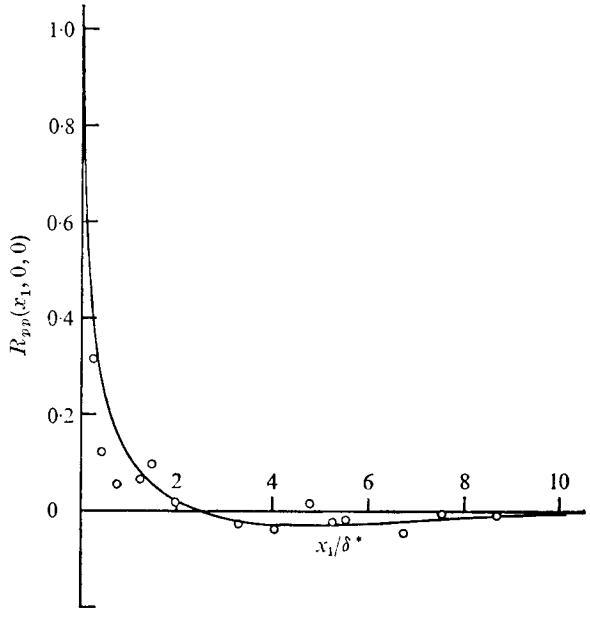

FIGURE 13. Streamwise wall pressure correlation. ○, present investigation, $\delta/a \simeq 4$; ——, Willmarth & Yang (1970), $\delta/a \simeq 2$.

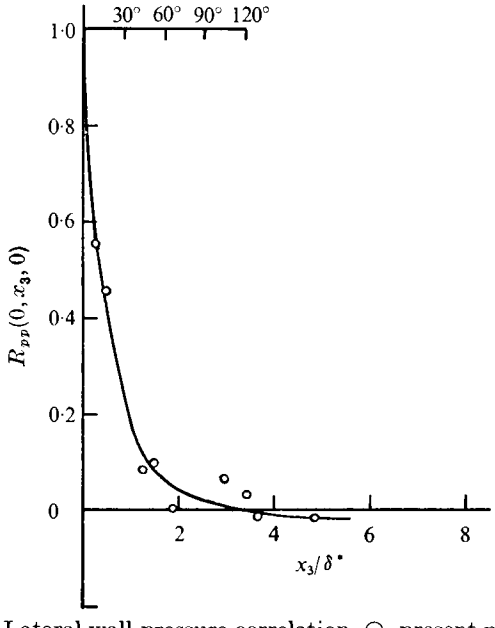

FIGURE 14. Lateral wall pressure correlation. ○, present measurements; ——, curve faired through present measurements.

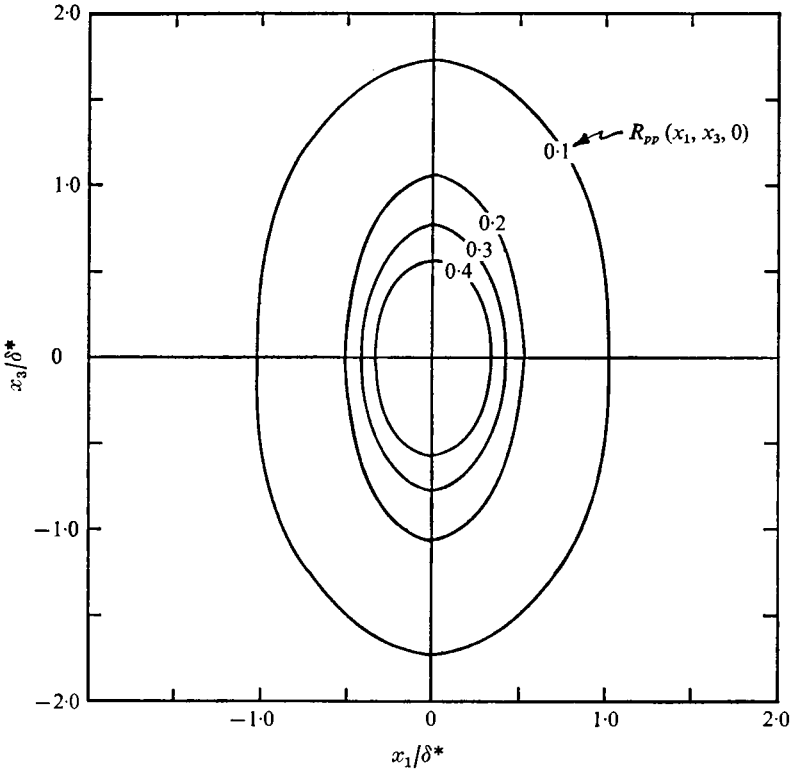

FIGURE 15. Contours of constant wall pressure correlation on the developed surface of the cylinder.

tions are correlated over a greater fraction of the cylinder circumference in the present case. The angular separation ϕ required to reach zero correlation for $\delta/a \simeq 4$ is more than twice that in the case $\delta/a \simeq 2$. This indicates that, as one proceeds downstream along the cylinder and δ/a increases, the pressure produced by larger eddies may eventually be appreciably correlated over the cylinder circumference.

Figure 15 shows the spatial extent of the contours of constant wall pressure correlation on the developed surface of the cylinder and includes oblique correlations not shown in figures 13 and 14. In terms of the displacement thickness the contours are very similar to those reported by Willmarth & Yang (1970) for a 3 in. cylinder with $\delta/a \simeq 2$. The contours are roughly circular as was observed by Willmarth & Yang (1970).

4.4. *Power spectrum of the wall pressure*

The dimensionless power spectrum of the wall pressure is displayed in figure 16 along with the measurements of Willmarth & Yang (1970). The results are similar but show a slightly increased spectral density in the range

$$1 < \omega\delta^*/U_\infty < 10.$$

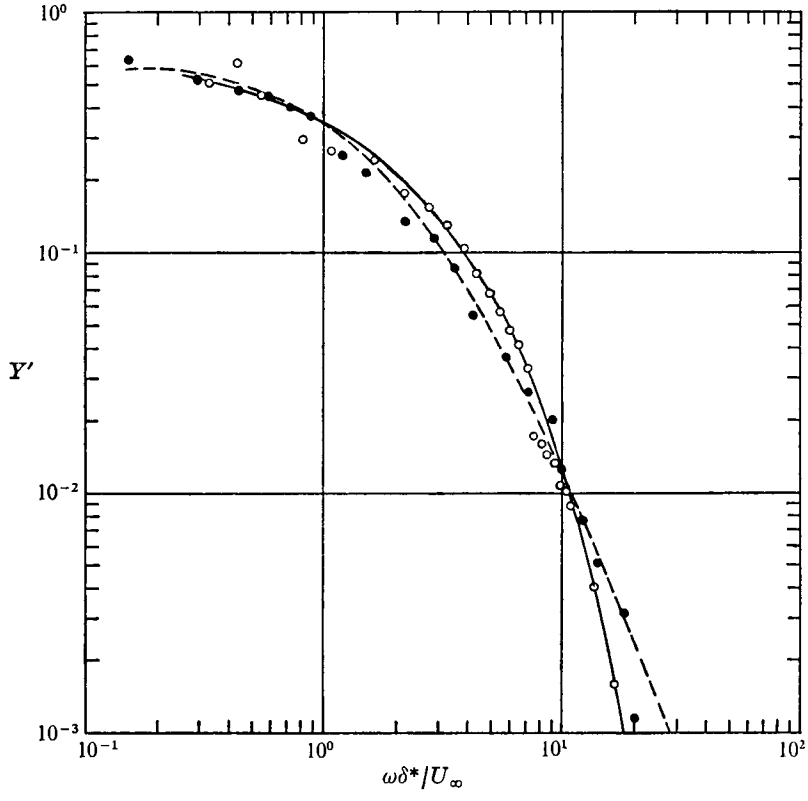

FIGURE 16. Dimensionless wall pressure spectra. The ordinate Y' is the power spectral density multiplied by U_∞ and divided by the product of mean-square wall pressure and displacement thickness. ○, present measurements, $\delta/a \simeq 4$; ●, Willmarth & Yang (1970), $\delta/a \simeq 2$.

For high frequencies the spectral density falls below the previous measurements for $\delta/a \simeq 2$. We have not attempted to correct these measurements for the loss of spatial resolution caused by the finite size of the transducers. It is now clear that none of the correction methods properly accounts for the very small scale pressure fluctuations that have been discovered by Blake, Emmerling & Hodgson using pin-hole microphones of small diameter; see Willmarth (1975*a*) for a discussion of these measurements.

The conclusion to be reached from these spectral measurements is that the increased transverse curvature of the present tests, with $\delta/a \simeq 4$, results in a further reduction in the size of the energy-containing small-scale eddies near the wall. In this context it should be noted that the transducer diameter (0·06 in.) is the same as in the previous measurements with $\delta/a \simeq 2$ (Willmarth & Yang 1970).

4.5. *Streamwise space–time correlation measurements in narrow frequency bands*

Let $p(x, z, t; \omega)$ be the signal obtained by passing the output of a pressure transducer at (x, z) through an ideal filter which has a narrow pass band centred at

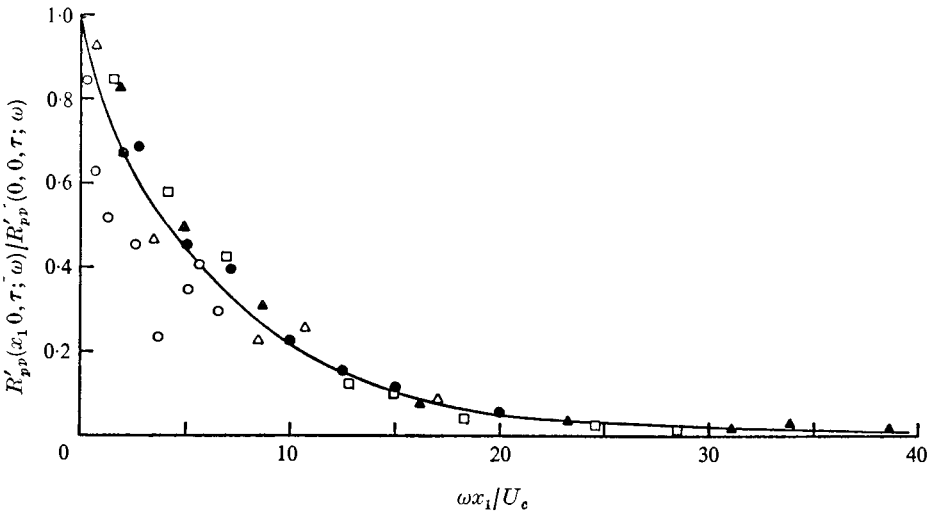

FIGURE 17. Narrow-band correlation coefficient for various frequency bands as a function of non-dimensional centre-frequency. ○, $500 < f < 630$ Hz; △, $1250 < f < 1600$ Hz; □, $2500 < f < 3160$ Hz; ▲, $3160 < f < 4000$ Hz; ●, $5000 < f < 6300$ Hz; ——, Willmarth & Yang (1970), with $\delta/a \simeq 2$.

a frequency ω and of width $\Delta\omega$. Then the correlation of pressure fluctuations measured by two pressure transducers a distance (x_1, x_3) apart at the central frequency ω for a bandwidth $\Delta\omega$ is

$$Q'_{pp}(x_1, x_3, \tau; \omega) = \frac{1}{T}\int_0^T \overline{p(x, z, t; \omega)\, p(x + x_1, z + x_3, t + \tau; \omega)}\, dt. \tag{9}$$

The narrow-band correlation coefficient is defined as

$$R'_{pp}(x_1, x_3, \tau; \omega) = Q'_{pp}(x_1, x_3, \tau; \omega)/Q'_{pp}(0, 0, 0; \omega). \tag{10}$$

Relatively narrow-band correlations of the wall pressure were measured in four frequency bands, with $x_3 = 0$. To carry out these measurements two Ithaco model 4213 variable band-pass filters were used. The high and low pass settings of the two filters were carefully matched to give a nearly identical phase shift as a function of frequency (within $\pm 3°$).

There is appreciable scatter in these measurements because not all the transducers in the array were similar in terms of their response to vibration. Reasonably accurate determinations of the decay rates of the envelopes of the peak correlation and of the time delay required to reach the peak correlation have been made. The convection speed was obtained in the manner described in §4.2 for the various frequency bands and spatial separations.

Figure 17 is a plot of the narrow-band correlation coefficient measured in various frequency bands as a function of dimensionless centre-frequency. The narrow-band correlation for the present case, $\delta/a \simeq 4$, is generally less than the values reported by Willmarth & Yang (1970) for $\delta/a \simeq 2$. The lowest values occur in the lower frequency bands. These results should be interpreted as they

were for a plane boundary layer, to indicate that the life-time of an eddy of given size is proportional to its size. See Willmarth (1975*a*) for a more complete discussion.

5. Summary and discussion of the measurements

We have described measurements of mean velocity profiles, wall shear stress for each profile and surface pressure fluctuations (in one case) within the turbulent boundary layer on circular cylinders which provide new information about the effect of transverse curvature on turbulent structure. One of the important results of these measurements is the fact that well-defined regions exist in which the two-dimensional law of the wall and a three-dimensional wake law are valid. We begin the discussion with the wall region.

In the wall region, the scaling of both the velocity and the distance from the wall are highly dependent upon the wall shear (or friction velocity), which in turn is a function of the Reynolds number and the cylinder diameter; see figure 8. It is apparent from figure 8 that in all cases the skin-friction coefficient increases as the cylinder diameter is decreased. Using the friction velocity determined from the measured wall shear stress the velocity profiles for the various cylinders were plotted in wall co-ordinates; see figure 5. From this figure it can be clearly seen that, for the cylinders with diameters in the range $\frac{1}{4}$ to 2 in., there is a well-defined profile extending very far from the wall which agrees with the two-dimensional law of the wall. It is also observed that, as the diameter of the cylinder decreases below $\frac{1}{4}$ in., the extent of this region decreases. However, even for the smallest cylinder tested, the profile continues to adhere to the two-dimensional law of the wall at smaller values of y^+ that are well outside the sublayer.

If the cylinder diameter is further reduced, the velocity profiles must eventually depart from the two-dimensional law of the wall within the sublayer region. Thus, as $a \to 0$ erosion of the conventional sublayer flow will occur. If we assume that the edge of the sublayer is at $y^+ = 5$ then in the present experiments at the smallest value of a^+ ($\simeq 33$) sublayer erosion does not yet occur. In fact, deviation from the two-dimensional profile occurs only at a relatively large value of y^+ of about 30 (i.e. $y^+ \simeq a^+$). If, for smaller cylinders, departure from the two-dimensional profile occurs at $y^+ \simeq a^+$ then erosion of the two-dimensional sublayer would occur at $y^+ \simeq a^+ \simeq 5$. One would attain the value $a^+ \simeq 5$ on a cylinder of diameter 0·0030 in. in air at the speeds we have used in this investigation. Measurements near the wall for cylinders of this diameter would not be possible by the hot-wire technique.

Rao (1967) has suggested that for a thick axisymmetric turbulent boundary layer the sublayer thickness will be comparable to the radius of transverse curvature. From the trend indicated by the present measurements (see figure 5) erosion of the sublayer, with a reduction in sublayer thickness, seems more likely as a^+ is reduced. In the present measurements for the smallest cylinder, with $a^+ \simeq 33$ and $\delta/a \simeq 40$, the sublayer is still present and coincides with the two-dimensional sublayer. The sublayer thickness is of the order of $\frac{1}{6}$ of the cylinder radius.

It is also of interest to consider the mean flow very near the surface. In this region the acceleration terms in the equations for the mean flow are negligible in comparison with the viscous terms. When there is no pressure gradient the shearing force $2\pi r\mu\,\partial U/\partial r$ per unit length upon a cylinder of fluid must be constant. This requires that the mean velocity be proportional to the logarithm of r. If we also require that $U = 0$ at $r = a$ we obtain

$$U/U^* = a^+ \ln(1 + y^+/a^+). \tag{11}$$

We have plotted (11) in figure 5 for the smallest value of a^+ in the present investigation ($a^+ = 33{\cdot}4$). Near the wall, i.e. for $y^+ < 4$, the velocity from (11) is not significantly different from the two-dimensional sublayer profile. This is also true in the sublayer for larger cylinders with $a^+ > 33{\cdot}4$ since (11) predicts a linear velocity profile near the wall. Significantly smaller values of the ratio U/U^* than those predicted by the two-dimensional law of the wall would occur within the sublayer for values of a^+ of the order of one. As already mentioned, measurements in air for small values of a^+ using hot wires are probably not possible. There are other experimental difficulties for values of a^+ of the order of one or less. To obtain turbulent flow at small values of a^+ the cylinder length l must be very large compared with the cylinder radius. In this case flow non-uniformities or disturbances in the free stream will be important. In other words the total shear force on the fluid at the cylinder surface becomes vanishingly small and does not dominate or control the flow. Measurements would require an exceptionally uniform cylinder and free-stream flow field.

As regards the law of the wake or defect law, the wakelike behaviour of the boundary layer on a cylinder is not as obvious when using wall co-ordinates as it is in the two-dimensional boundary layer. It is known that for the two-dimensional case the profiles rise above the logarithmic portion of the law of the wall for large y^+. However, it is observed from figure 5 that for the cylinders of smaller diameter the profiles depart from the logarithmic portion by falling below it. Yet, in analogy with two-dimensional flow with zero pressure gradient, the wakelike outer flow should obey a defect law. Thus, in accordance with (6), the velocity defect has been plotted as a function of y/δ in figure 9. This figure indicates that, as the value of δ/a becomes small, the defect profiles approach the flat-plate universal data, as one would expect.

The present measurements strongly support the extended law of the wall and the defect law set forth in (4)–(6). However, additional measurements for different values of the boundary-layer thickness, cylinder diameter and friction velocity are needed in order to determine completely the functional dependence indicated by (4)–(6). In future investigations of the mean flow in axisymmetric turbulent boundary layers, experiments should be designed to provide sufficient data concerning the effects of transverse curvature to allow a complete empirical formulation of the mean flow field. This was possible in the two-dimensional case only after sufficient data and understanding had accumulated; see Clauser (1956) and Coles (1955, 1956).

The measurements also provide some information about the question of reversion to laminar flow when the cylinder diameter is reduced. Patel (1973)

has predicted that below a certain cylinder radius, $a^+ = 28$, the boundary layer should be transitional and not fully turbulent. In the present measurements there does not appear to be any tendency towards relaminarization since the measured shear stress on the 0·02 in. cylinder at the lowest value of a^+, $a^+ = 33{\cdot}4$, is somewhat more than a factor of 6 larger than the laminar value that is predicted at 18·3 ft on the 0·02 in. cylinder from the theory of Glauert & Lighthill (1955). In addition, the velocity profile measurements displayed in figures 5 and 9 show consistent behaviour as the cylinder radius is reduced. The velocity defect becomes smaller at any given value of y/δ and the departure from the extended law of the wall occurs at progressively smaller values of y^+. Furthermore, the velocity fluctuations observed during the mean profile measurements using hot wires were not intermittent in the wall region.

Patel's (1973) prediction is based upon the supposition that, since the boundary-layer profiles on a cylinder with no pressure gradient and on a two-dimensional surface in a favourable pressure gradient are very full, they are similar in their behaviour with respect to relaminarization. He predicted the value $a^+ \simeq 28$ for relaminarization of the boundary layer on a cylinder by requiring that his stress-gradient parameter above the sublayer should be the same as that observed during relaminarization of a plane boundary layer. The supposition that the boundary-layer profile on a cylinder is very full is indeed found to be true; see figure 9. However, this is a result of the cylindrical geometry of the flow. In a cylinder boundary layer there is no acceleration of the free stream, which in two-dimensional flow is directly responsible for the favourable pressure gradient which produces a full velocity profile.

Willmarth (1975*b*) has proposed a mechanism for the cyclic occurrence of bursts in a plane boundary layer which may be useful in understanding the difference between the turbulent production mechanisms in a plane boundary layer with a favourable pressure gradient and a boundary layer on a cylinder with zero pressure gradient. The pressure field from the large eddies in the outer flow is thought to produce a massaging action on the sublayer flow and prepare it for the occurrence of a burst. The massaging action of the large eddies passing over the sublayer is presumed to create, during random periods of time, an unstable inflexional profile in localized regions near the wall. Bursts which generate new turbulence occur in these regions of locally unstable inflexional profiles. When there is a very favourable pressure gradient the outer flow containing the large eddies is strongly accelerated. The result of this rapid acceleration is that the large eddies pass more quickly over the sublayer flow field, so that their massaging action at a given point near the wall has a greatly reduced time scale. Then the flow near the wall is locally more stable since the degree of instability and therefore the number of locally unstable regions in the sublayer are reduced. The result is that the number and intensity of bursts are also reduced. Ultimately, a reversion to laminar flow occurs.

In the boundary layer on a cylinder with zero pressure gradient the structure of turbulence is of approximately uniformly reduced scale as discussed by Willmarth & Yang (1970). Willmarth & Yang have also shown, in agreement with the present measurements of turbulent pressure fluctuations, that the relation-

ship between the convection velocities of the various scales of turbulence remains the same as it is in a plane boundary layer with zero pressure gradient. Therefore, it is suggested that in the boundary layer on a cylinder with zero pressure gradient there is no reduction in the time scale of the massaging action of the larger eddies on the sublayer flow relative to the time scale for the sublayer flow field. The general mechanism for the cyclic recurrence of bursts of newly generated turbulence is presumably not greatly affected by the 'fullness' of the velocity profile caused by the cylindrical flow geometry at least for the conditions that we have studied, $a^+ \geqslant 33{\cdot}4$.

As regards the wall pressure fluctuation measurements, most of the measurements made by Willmarth & Yang (1970) were repeated. The techniques and equipment were similar too. The primary difference was that the measurements were made on a smaller cylinder of diameter 1 in., which resulted in $\delta/a \simeq 4$. The results showed that the measurements were in substantial agreement with the previous work of Willmarth & Yang (1970) on a 3 in. cylinder for $\delta/a \simeq 2$.

The turbulent pressure-producing eddies and therefore the turbulent length and time scales for the 1 in. cylinder are slightly smaller when compared with the displacement thickness than those for the 3 in. cylinder. The conclusion reached by Willmarth & Yang (1970) that there are two primary effects in a boundary layer with transverse curvature that reduce the size of turbulent eddies relative to those in a plane boundary layer remains valid. These effects were caused by the increased 'fullness' of the velocity profile and by the limited lateral extent of the axisymmetric boundary layer. The 'fullness' of the profile causes eddies moving at a given convection speed to be of reduced size because a given mean speed is attained at a smaller distance from the wall. The limited lateral extent of the axisymmetric turbulent boundary layer (for $\delta/a \rightarrow \infty$ this is 2δ) results in a lateral shearing action by the free stream on the larger eddies when they extend or move laterally.

The present measurements also show that, as δ/a increases, the large-scale surface pressure fluctuations are correlated over a greater fraction of the cylinder circumference (see figure 14) compared with the measurements of Willmarth & Yang (1970) for $\delta/a \simeq 2$. In the case of a plane boundary layer the larger eddies are completely bounded on one side by the plane wall. In an axisymmetric boundary layer the outer perimeter of the larger eddies is very large compared with the inner perimeter near the wall. Thus, when δ/a is large the structure and evolution of the larger eddies (once they have been created) do not depend directly upon the presence of the wall.

The support of the Office of Naval Research and the encouragement of Mr Hugh Fitzpatrick during the course of this research are gratefully acknowledged.

Appendix. Construction of small hot-wire anemometer

The material used to construct the hot-wire probe is an alloy 90 % platinum and 10 % rhodium fabricated by the Wollaston process. The Wollaston wire consists of a thin filament of the above alloy (0·5 μm in diameter) encased in a silver jacket. A length of this wire is cut and bent into the shape of a U by holding it over a piece of shim stock whose edges have been rounded. The radius of curvature of the U must be large compared with the desired sensitive length of the probe to ensure that the sensitive length of the wire is relatively straight. To obtain a straight wire the bottom of the U may be flattened. With the aid of a stereoscopic microscope and a micromanipulator, the legs of the U are soldered onto the prongs of a conventional probe. A 10 W soldering iron with the nib ground to a fine point is used. It is convenient to hold the wire by a piece of tape at the bend while soldering is being done. Care must be taken to relieve any tension in the wire after the tape is removed by softening one of the solder joints. The probe is cleaned with trichlorethylene to remove grease and residual adhesive left from the tape.

The U-shaped end of the wire is next dipped into a capillary tube containing a dilute (60 %) nitric acid such that about two-thirds of its length is submerged. It is then slowly withdrawn, causing the silver jacket to taper towards the bend. The etching process is then stopped by washing the probe in water. A smaller capillary, just large enough to admit the bend of the U, is used to etch away the silver at the bend until the desired length of wire is exposed. The probe is then washed with water and trichloroethylene and is ready for use. If the curvature of the sensitive length of the wire is too great, the probe may be rotated until the plane of the U is vertical and the lower solder joint softened, allowing the weight of the silver jacket to pull the wire straight. Figure 4 (plate 1) is a Polaroid photograph of a typical probe taken with a scanning electron microscope.

The probes are quite fragile. The environment in which they are used must be free from dust and vibration. They have been operated successfully in air flows with velocities as high as 250 ft/s. The process of etching the silver jacket, which acts as the probe support, can easily be controlled, allowing the probe to be positioned very close to the wall.

REFERENCES

Cebeci, T. 1970 Laminar and turbulent incompressible boundary layers on slender bodies of revolution in axial flow. *J. Basic Engng, Trans. A.S.M.E.* D **92**, 545.

Chase, D. M. 1972 Mean velocity profile of a thick turbulent boundary layer along a long cylinder. *A.I.A.A. J.* **10**, 849.

Clauser, F. H. 1956 The turbulent boundary layer. *Adv. Appl. Mech.* **4**, 1.

Coles, D. E. 1955 The law of the wall in turbulent shear flow. 50 *Jahre Grenzschicht-forschung*, p. 153. Braunschweig: F. Vieweg.

Coles, D. E. 1956 The law of the wake in a turbulent boundary layer. *J. Fluid Mech.* **1**, 191.

Glauert, M. B. & Lighthill, M. J. 1955 Axisymmetric boundary layer on a long thin cylinder. *Proc. Roy. Soc.* A **203**, 188.

MOORE, F. K. 1952 Displacement effect of a three-dimensional boundary layer. *N.A.C.A. Tech. Note*, no. 2722.

PATEL, V. C. 1965 Calibration of a Preston tube and limitations on its use in pressure gradients. *J. Fluid Mech.* **23**, 185.

PATEL, V. C. 1973 A unified view of the law of the wall using mixing-length theory. *Aero. Quart.* **24**, 55.

PRESTON, J. H. 1954 The determination of turbulent skin friction by means of Pitot tubes. *J. Roy. Aero. Soc.* **58**, 109.

RAO, G. N. V. 1967 The law of the wall in a thick axisymmetric turbulent boundary layer. *J. Appl. Mech.* **34**, 237.

RAO, G. N. V. & KESHAVAN, N. R. 1972 Axisymmetric turbulent boundary layers in zero pressure gradient flows. *J. Appl. Mech.* **39**, 25.

REID, R. O. & WILSON, B. W. 1963 Boundary flow along a circular cylinder. *J. Hydraul. Div., Proc. A.S.C.E.* **3**, 21.

RICHMOND, R. L. 1957 Experimental investigation of thick axially symmetric boundary layers on cylinders at subsonic and hypersonic speeds. Thesis, California Institute of Technology. (See also *Hypersonic Res. Proj. Memo.* no. 39.)

WHITE, F. M. 1972 An analysis of axisymmetric turbulent flow past a long cylinder. *J. Basic Engng, Trans. A.S.M.E.* D **94**, 200.

WHITE, F. M., LESSMANN, G. H. & CHRISTOPH, G. H. 1973 Skin friction in thick axisymmetric boundary layers. *A.I.A.A. J.* **11**, 6, 821.

WILLMARTH, W. W. 1975*a* Pressure fluctuations beneath turbulent boundary layers. *Ann. Rev. Fluid Mech.* **7**, 13.

WILLMARTH, W. W. 1975*b* Structure of turbulence in boundary layers. *Adv. Appl. Mech.* **15**, 159.

WILLMARTH, W. W., WINKEL, R. E., BOGAR, T. J. & SHARMA, L. K. 1975 Axially symmetric turbulent boundary layers on cylinders. *Dept. Aerospace Engng, Univ. Michigan, Rep.* no. 021490-3-T.

WILLMARTH, W. W. & YANG, C. S. 1970 Wall pressure fluctuations beneath turbulent boundary layers on a flat plate and a cylinder. *J. Fluid Mech.* **41**, 47.

WILLS, J. A. B. 1962 The correction of hot-wire readings for proximity to a solid boundary. *J. Fluid Mech.* **12**, 388.

YU, Y. S. 1958 Effect of transverse curvature on turbulent-boundary-layer characteristics. *J. Ship Res.* **3**, 33.

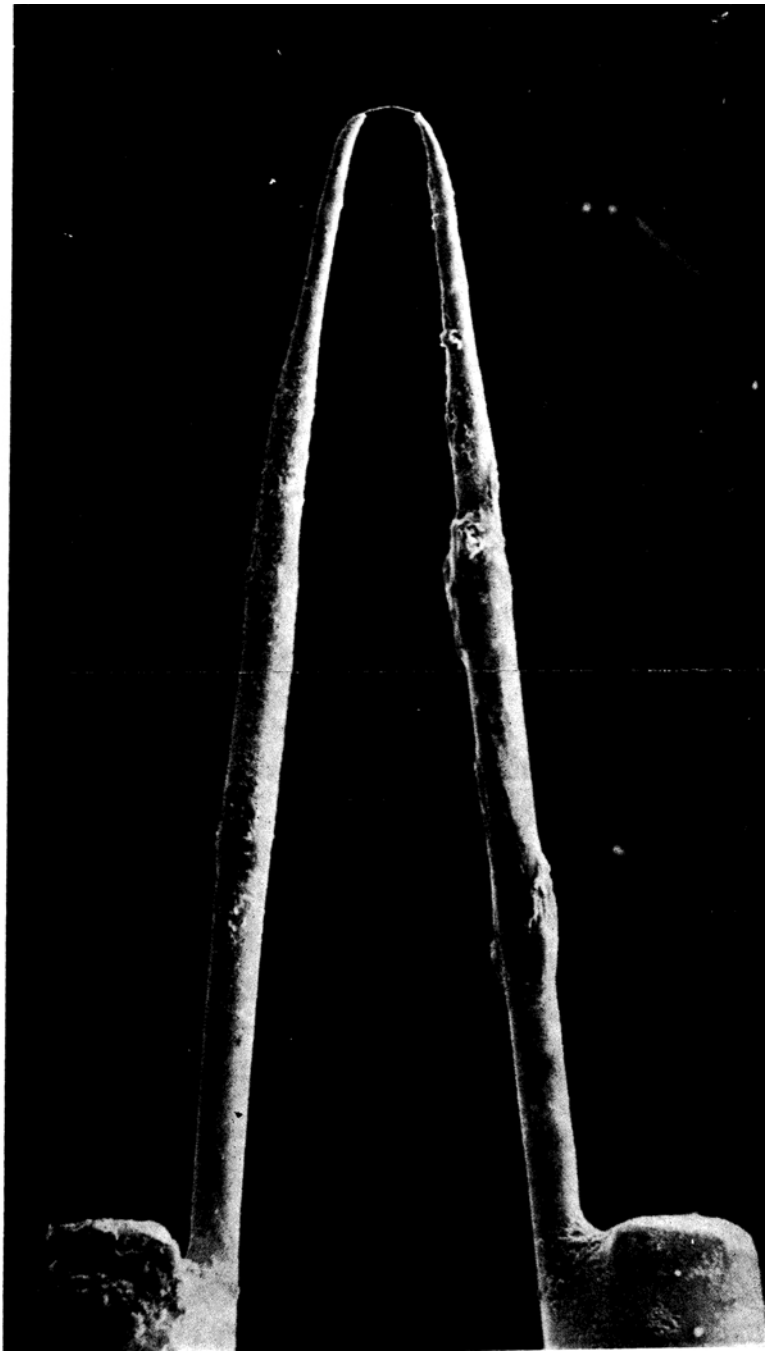

FIGURE 4. Scanning electron microscope photograph of a typical hot wire used in the investigation; length of active element = 100 μm, diameter of active element = 0·5 μm.